Disturbance Observer-Based Pitch Control of Wind Turbines for Enhanced Speed Regulation

Yuan Yuan
Department of Mechanical Engineering,
University of Connecticut,
Storrs, CT 06269

X. Chen
Assistant Professor
Department of Mechanical Engineering,
University of Connecticut,
Storrs, CT 06269

J. Tang[1]
Professor
Department of Mechanical Engineering,
University of Connecticut,
Storrs, CT 06269
e-mail: jtang@engr.uconn.edu

Time-varying unknown wind disturbances influence significantly the dynamics of wind turbines. In this research, we formulate a disturbance observer (DOB) structure that is added to a proportional-integral-derivative (PID) feedback controller, aiming at asymptotically rejecting disturbances to wind turbines at above-rated wind speeds. Specifically, our objective is to maintain a constant output power and achieve better generator speed regulation when a wind turbine is operated under time-varying and turbulent wind conditions. The fundamental idea of DOB control is to conduct internal model-based observation and cancelation of disturbances directly using an inner feedback control loop. While the outer-loop PID controller provides the basic capability of suppressing disturbance effects with guaranteed stability, the inner-loop disturbance observer is designed to yield further disturbance rejection in the low frequency region. The DOB controller can be built as an on–off loop, that is, independent of the original control loop, which makes it easy to be implemented and validated in existing wind turbines. The proposed algorithm is applied to both linearized and nonlinear National Renewable Energy Laboratory (NREL) offshore 5-MW baseline wind turbine models. In order to deal with the mismatch between the linearized model and the nonlinear turbine, an extra compensator is proposed to enhance the robustness of augmented controller. The application of the augmented DOB pitch controller demonstrates enhanced power and speed regulations in the above-rated region for both linearized and nonlinear plant models.
[DOI: 10.1115/1.4035741]

Keywords: disturbance observer based control, wind turbine, generator speed regulation, disturbance rejection

1 Introduction

Wind energy is one of the most promising renewable energy sources in the world. To efficiently harvest the wind kinetic energy, modern wind turbines are designed to have large sizes and flexible structures. Such system properties, however, also create a major challenge for long-term durability of wind turbines. In the meantime, the operating wind field is often highly turbulent, which gives rise to significant fluctuation of plant dynamics and hence compromises the turbine performance. Based on the wind speed, the operation of wind turbines can be divided into three regions. In region 1, wind turbines do not start up until the wind speed reaches a threshold value (i.e., the cut-in speed). In region 2 (below-rated), torque control is often applied to capture the maximum power from wind. In region 3 when wind speed is sufficiently high (above-rated), wind turbines need to operate at rated speed and provide constant rated power output.

In the above-rated region, pitch control is commonly implemented to avoid the over-speed of rotor. In this process, the highly nonlinear nature of a wind turbine calls for a robust and intelligent control system to tackle the time-varying turbulent wind field. Since the plant model is sensitive to wind speed, a collective proportional-integral-derivative (PID) controller has been developed to regulate the generator speed where a gain scheduled part is added in order to deal with the aerodynamic sensitivity change of the wind speed (which is treated as the baseline controller for comparison in this research) [1]. The optimal power and speed in region 3 under time-varying wind field may then be realized with unknown model parameters. By linearizing the nonlinear wind turbine model under selected operating point, a linear turbine model can be obtained to formulate the state-space feedback control for speed regulation. As the wind speed is generally unpredictable without proper sensor, disturbance accommodating control (DAC) has been adopted to facilitate disturbance rejection and mitigate loads by estimating wind speed with additional state estimators [2,3]. However, the estimator accuracy is not usually guaranteed. Since the linearized model is dependent upon the operating point, adaptive control has been attempted to achieve better speed regulation than the PID method, as wind turbine model parameters are not precisely known [4]. With the recent development of light detection and ranging (LIDAR), feedforward strategy can be adopted to reject the varying wind disturbance to obtain better rotor speed tracking and further mitigate structural loads. In Ref. [5], wind velocity is captured by LIDAR and fed to a filtered-x recursive least square algorithm, which cancels the disturbance effect.

In wind turbines, one of the major challenges for control development comes from the time-varying external wind disturbances [3,5,6]. It is worth noting that in the field of high precision motion control, the concept of disturbance observer (DOB)-based control with internal model principle has been recently explored to reject disturbances with unknown and/or time-varying spectra [7]. For example, a DOB-based algorithm has been formulated and implemented to a wafer-scanning process in lithography [8]. The fundamental idea of DOB control is to conduct an internal disturbance observation using model inversion and then to achieve disturbance cancelation by using an inner feedback control loop. As such, the potential effectiveness of DOB control for wind turbine applications is promising, since it may reject wind disturbances in speed regulation without requiring real-time sensor such as LIDAR. In comparison, the disturbance compensation in DAC [2] is facilitated by minimizing the norm of disturbance function $(BG_d + B_d\Theta)$.[2] The performance of DAC would thus be limited if the disturbance rejection function does not have full rank.

[1]Corresponding author.

Contributed by the Dynamic Systems Division of ASME for publication in the Journal of Dynamic Systems, Measurement, and Control. Manuscript received May 5, 2016; final manuscript received December 29, 2016; published online May 9, 2017. Assoc. Editor: Ryozo Nagamune.

In this research, we formulate a DOB-based control scheme for wind turbines, aiming at asymptotically rejecting disturbances at above-rated wind speeds. Specifically, our objective is to maintain a constant output power and achieve better generator speed regulation when the wind turbine is operated under time-varying and turbulent wind conditions. The DOB structure consists of a usual PID controller augmented with an inner loop feedback. While the outer-loop PID controller provides the basic capability of suppressing disturbance effects with guaranteed stability, the inner-loop DOB (i.e., the Q filter) is designed to yield further disturbance rejection in the low frequency region and at the same time maintain the original capability of the PID controller in terms of suppressing disturbance effects in the high frequency region. Although disturbance rejection through disturbance estimation with a traditional state estimator is well known [2,3,9], the DOB structure formulated in this research allows simple and intuitive tuning of the inner DOB loop gains that are independent of the outer-loop state feedback or PID gains [10]. The DOB controller may therefore be built as an on–off loop that is independent of the original control loop employed in existing wind turbines. This add-on feature makes it easy to be implemented and validated in existing wind turbines. In practice, owing to the model mismatch, applying the DOB that is designed from the linearized model to the actual, nonlinear system may not lead to desired performance especially system stability. An extra compensator is then proposed to enhance the robustness of the augmented controller, which can not only ensure the stability but also widen the disturbance rejection bandwidth. The new algorithm is applied to both linearized and nonlinear National Renewable Energy Laboratory (NREL) offshore 5-MW baseline wind turbine models.

The rest of this paper is organized as follows: We start with a brief discussion of the 5-MW wind turbine model in Sec. 2, followed by the formulation of the DOB based control in Sec. 3. The results and discussion are presented in Sec. 4, where DOB will exhibit better generator speed regulation as well as stability robustness in a wide region of wind speeds. Concluding remarks are summarized in Sec. 5.

2 Model Description

In this research, we employ the NREL offshore 5-MW turbine for control development, which is a benchmark wind turbine widely used in control studies [1,4,11]. It is a three-bladed upwind variable-speed variable blade-pitch-to-feather-controlled horizontal axis turbine [1]. The rotor diameter is 126 m, and the hub height is 90 m. The cut-in wind speed is 3 m/s, the rated wind speed is 11.4 m/s, and the cut-out wind speed is 25 m/s. The rated generator speed is 1173.7 rpm.

A variable-speed wind turbine generally consists of blades, a tower, a nacelle, a hub, drivetrain shafts, a gearbox, and a generator. The aerodynamic power captured by the rotor is given as [2]

$$P_{\text{wind}} = \frac{1}{2}\rho\pi R^2 C_p(\lambda,\beta)v^3 \tag{1}$$

where R is the rotor radius, and ρ is the air density. The power coefficient C_p is a nonlinear function of tip speed ratio λ and pitch angle β, and can be obtained from look-up table generated by field test data. Here

$$\lambda = \frac{\omega R}{v} \tag{2}$$

where v is the wind speed, and ω is the rotor speed. From Eqs. (1) and (2), we can observe that the aerodynamic power P_{wind} depends on wind speed, rotor speed, and blade pitch angle. Pitch angle control is therefore the key to adjust the aerodynamic power captured by rotor to achieve speed regulation. The aerodynamic torque applied to the rotor can be expressed as [2]

$$T_a = \frac{\pi C_p(\lambda,\beta)\rho R^2 v^3}{2\omega} \tag{3}$$

The nonlinear aero-elastic equation of motion for the turbine has the following form [12]:

$$\mathbf{M}(\mathbf{q},\mathbf{u},t)\ddot{\mathbf{q}} + \mathbf{f}(\mathbf{q},\dot{\mathbf{q}},\mathbf{u},\mathbf{u}_d,t) = 0 \tag{4}$$

where $\mathbf{M}$ is the mass matrix, $\mathbf{f}$ is the nonlinear forcing function vector that contains the stiffness and damping effects, $\mathbf{q}$ is the response vector, $\mathbf{u}$ is the vector of control inputs, $\mathbf{u}_d$ is the vector of wind input disturbance, and t is time. In this research, we use the fatigue, aerodynamics, structures, and turbulence (FAST) code developed by NREL [12] to establish the numerical model of the wind turbine. Without the loss of generality, we let the following degrees-of-freedom (DOFs) be switched on in FAST: the first flapwise blade mode DOF (of three blades), the generator DOF, and the drivetrain torsional flexibility DOF.

Using FAST, we can linearize Eq. (4) by perturbing each variable about its corresponding operating point [2,12]. Following the usual simplification performed in literature [2,3,11], we eliminate the generator azimuth state and reduce the flapwise mode of three blades to one symmetric mode. We then cast the linearized equation of motion into the state-space representation

$$\dot{\mathbf{x}} = \mathbf{A}\mathbf{x} + \mathbf{B}\Delta\mathbf{u} + \mathbf{B}_d\Delta\mathbf{u}_d \tag{5a}$$

$$\mathbf{y} = \mathbf{C}\mathbf{x} + \mathbf{D}\Delta\mathbf{u} + \mathbf{D}_d\Delta\mathbf{u}_d \tag{5b}$$

where $\mathbf{x}$ is a five-dimension state vector, x_1 is the drive-train torsional deflection perturbation, x_2 is the rotor first symmetric flap displacement perturbation, x_3 is the generator speed perturbation, x_4 is the drive-train torsional velocity perturbation, and x_5 is the rotor first symmetric flap velocity perturbation. $\mathbf{A}$ is the state matrix, $\mathbf{B}$ is the control input matrix, $\mathbf{B}_d$ is the disturbance input matrix, $\mathbf{C}$ is the output matrix, $\mathbf{D}$ is the control input transmission matrix, $\mathbf{D}_d$ is the wind input disturbance transmission matrix, $\Delta\mathbf{u}$ is the control input (i.e., the perturbed blade collective pitch angle), $\Delta\mathbf{u}_d$ is the disturbance input (i.e., the perturbed wind speed), and $\mathbf{y}$ is the output.

Usually, the generator speed can be regulated by the aerodynamic torque T_a (Eq. (3)) and the generator torque denoted as T_g. There are two separate single-input and single-output control loops which are the torque controller and the blade pitch controller. In the below-rated region, the torque controller is used to govern the generator speed, while blade pitch angle is held constant to maintain the maximum aerodynamic coefficient C_p. In the above-rated region, the pitch controller is used to limit the aerodynamic torque T_a to avoid extreme loads. The operating point for linearization in this research is chosen to be wind speed $v = 18$ m/s, pitch angle $\theta = 14.92$ deg, and rotor speed $\omega_r = 12.1$ rpm. We choose $v = 18$ m/s because it is in the middle between the cut-in speed (11.4 m/s) and the cut-out speed (25 m/s). $\theta = 14.92$ deg is the corresponding blade pitch angle that produces the rated power, and $\omega_r = 12.1$ rpm is the rated rotor speed.

3 Control Design

In this research, we adopt the torque controller designed in Ref. [1] for the same NREL offshore 5-MW baseline wind turbine. Here, in this section, we formulate the DOB-based pitch controller. We assume that the generator speed is the only measurement available, and that the controller gives the collective pitch command. The pitch actuator dynamics is assumed to be first-order, since the actuator inertia is negligible compared to those of other

[2] B is the control input matrix, G_d is the disturbance state gain, B_d is the wind disturbance input matrix, and Θ is the output matrix in disturbance wave generator.

components. We employ pitch angle saturation and pitch rate limiter to meet the hardware limitations.

3.1 Disturbance Rejection in Disturbance Observer-Based Control. As mentioned in Sec. 1, in order to deal with the time-varying turbulent wind condition, Jonkman et al. developed a gain scheduled PID type control, hereafter referred to as the gain scheduled proportional integral (GSPI) control [1]. The gain-scheduling part is derived based on the pitch sensitivity which is expressed as the sensitivity of the aerodynamic power to the rotor collective blade pitch. It is worth noting that the relation between the pitch sensitivity and the pitch angle, strictly speaking, is not linear. Thus, the disturbance effects may not be perfectly canceled. Here, we propose to incorporate a disturbance observer structure to a traditional PID controller to fundamentally enhance the disturbance rejection performance. In this structure, while the outer-loop PID controller provides the basic capability of suppressing disturbance effects with guaranteed stability, an inner-loop disturbance observer (i.e., the Q filter) is designed to yield further disturbance rejection in the low frequency region and at the same time maintain the original capability of the PID controller in terms of suppressing disturbance effects in the high frequency region.

The disturbance observer will lead to an inverse-based disturbance rejection scheme, as shown in Fig. 1. Two discrete transfer functions can be obtained from Eq. (5) to represent the model from perturbed blade pitch angle to perturbed generator speed ($P(z^{-1})$) as well as the model from perturbed wind speed to perturbed generator speed ($P_d(z^{-1})$), respectively. The outer-loop feedback controller is a PID controller $C(z^{-1})$. The inner-loop feedback controller, depicted as the collection of blocks connected through thick arrows in Fig. 1, is the DOB, which is an internal feedback of the disturbance $d_0(k)$.

We lump all the input disturbances to $d(k)$, and focus on the signal flow from $d(k)$ to $\hat{d}(k)$. If $P_n^{-1}(z^{-1})$ is the exact model inversion of plant $P(z^{-1})$, letting the filter $Q(z^{-1}) = 1$ will create the exact disturbance estimation of $d(k)$, which will result in the perfect disturbance rejection at the input of the plant. We then consider the flows of control input $u(k)$. Practically, $P^{-1}(z^{-1})$ is acausal. We thus introduce $P_n^{-1}(z^{-1}) = z^{-m}P^{-1}(z^{-1})$. z^{-m} is added to make it causal and implementable (i.e., the degree of numerator not exceeding the degree of denominator), where m is the relative degree of $P(z^{-1})$. We can have $P_n^{-1}(z^{-1}) \cdot P(z^{-1}) = z^{-m}$, which means $u(k)$ will not influence $\hat{d}(k)$ [7]. Consequently, the raw disturbance estimation $d_r(k)$ includes rich information of $d(k)$ with the introduction of the inverse architecture. Nevertheless, in practical cases we usually have $P_n^{-1}(z^{-1}) \cdot P(z^{-1}) \approx z^{-m}$, and thus, $d_r(k) \approx z^{-m}d(k)$. Mismatch exists between $d_r(k)$ and $d(k)$, because $d_r(k)$ is a delayed estimate of $d(k)$. In what follows we demonstrate how this issue can be handled.

Consider the original problem of wind turbine generator speed tracking. The signal $d_0(k)$ is the time-varying wind disturbance, which will go through a disturbance model $P_d(z^{-1})$ to affect the input of the plant. $r(k)$ is the setpoint, $u(k)$ is the pitch angle, and $y(k)$ is the generator speed. When $P(z^{-1})$ is the linearized model, these signals become the perturbed values corresponding to the operating point. The signal $\hat{d}(k)$ is a negative internal feedback of disturbance to cancel out the influence of $d(k)$. When disturbance $d(k)$ enters the plant directly, we can observe, from Fig. 1, that

$$\begin{aligned} d(k) - \hat{d}(k) &= d(k) - Q(z^{-1})P_n^{-1}(z^{-1})P(z^{-1})(d(k) + u(k)) \\ &\quad + Q(z^{-1})z^{-m}u(k) \\ &\approx [1 - z^{-m}Q(z^{-1})]d(k) \end{aligned} \tag{6}$$

Let $A_d(z^{-1})$ and $B_d(z^{-1})$ be the denominator and numerator of the z transform of disturbance source, respectively. For a disturbance that satisfies the following condition in the asymptotic sense:

$$A_d(z^{-1})d(k) = B_d(z^{-1})\delta(k) = 0 \tag{7}$$

we can achieve disturbance rejection if [7]

$$1 - z^{-m}Q(z^{-1}) = K(z^{-1})\frac{A_d(z^{-1})}{A_d(\alpha z^{-1})} \tag{8}$$

where $K(z^{-1})$ is a polynomial of z^{-1} to assure causality, $A_d(\alpha z^{-1})$ is a polynomial in which all z^{-1} in $A_d(z^{-1})$ are replaced by αz^{-1}, $\alpha \in (0, 1)$. The form of $A_d(z^{-1})$ depends on the disturbance form and the interested frequency region. To deal with the wind disturbance and to ensure the stability of the augmented system (which is not always guaranteed due to the possible model mismatch in practice), the Q filter needs to be carefully selected, which will be further discussed in details in Sec. 3.3 based on the stability and robustness criteria.

In certain conventional cases such as vibration mitigation in precision manufacturing, the disturbance frequency is either known or can be adaptively identified. For disturbance in wind turbines, however, it is generally difficult to find or define its specific frequency contents, since the highly random wind can contain many frequencies. To determine $A_d(z^{-1})$, we model the wind disturbance through the following disturbance wave generator [2]:

$$\dot{\mathbf{z}}_d = \mathbf{F}\mathbf{z}_d \tag{9a}$$

$$\mathbf{u}_d = \mathbf{\Theta}\mathbf{z}_d \tag{9b}$$

Any waveform governed by a linear ordinary differential equation can be expressed by this generator. We assume that the wind disturbance is the variance from the wind speed at the operating point and has a known waveform but unknown amplitude. Specifically, we can model it as step disturbance. $\mathbf{F}$ and $\mathbf{\Theta}$ are assumed to be known as

$$\mathbf{F} \equiv 0 \tag{10a}$$

$$\mathbf{\Theta} \equiv 1 \tag{10b}$$

If we take the z transform of the step disturbance and treat the disturbance as the response to an impulse input $\delta(k)$, we can obtain

$$d_0(k) = \frac{M(k)}{1 - z^{-1}}\delta(k) \tag{11}$$

where owing to the time-varying nature, an unknown magnitude $M(k)$ is added.

When disturbance enters through a disturbance model $P_d(z^{-1}) = B_{p,d}(z^{-1})/B_p(z^{-1})$, the output will be $y(k) = P_d(z^{-1})P(z^{-1})d_0(k) + P(z^{-1})u(k)$ as shown in Fig. 1, and the disturbance entering the plant is

$$d(k) = P_d(z^{-1}) \cdot d_0(k) = \frac{M(k)}{1 - z^{-1}}\frac{B_{p,d}(z^{-1})}{B_p(z^{-1})}\delta(k) \tag{12}$$

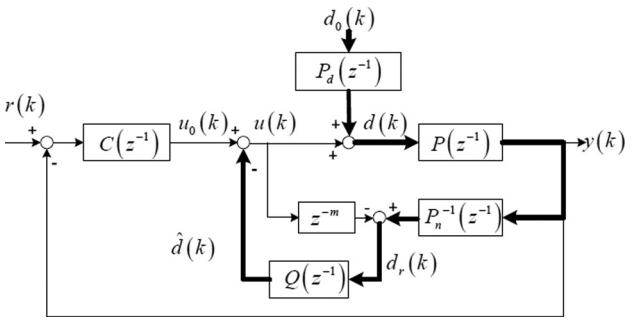

Fig. 1 Structure of the DOB-based control

Thus, we have, asymptotically

$$\frac{(1-z^{-1})B_p(z^{-1})}{M(k)}d(k) = B_{p,d}(z^{-1})\delta(k) = 0 \tag{13}$$

Recall Eqs. (7) and (8). Based on the internal model principle [13], to asymptotically reject the disturbance, the following equation should be satisfied:

$$1 - z^{-m}Q(z^{-1}) = \frac{(1-z^{-1})B_p(z^{-1})}{M(k)} \tag{14}$$

To further ensure the causality and the capability of local loop shaping, filters $K(z^{-1})$ and $\bar{B}_p(\beta z^{-1})$ are added to the right-hand side of Eq. (14)

$$1 - z^{-m}Q(z^{-1}) = \frac{\bar{B}_p(z^{-1})}{M(k)}\frac{K(z^{-1})}{\bar{B}_p(\beta z^{-1})} \tag{15}$$

It is worth noting that Eq. (13) still holds after those two filters are introduced. $K(z^{-1})$ is selected as a finite impulse response (FIR) filter $K(z^{-1}) = k_0 + k_1 z^{-1} + \cdots + k_{n_k} z^{-n_k}$, and

$$\bar{B}_p(z^{-1}) = (1-z^{-1})B_p(z^{-1}) \tag{16a}$$

$$\bar{B}_p(\beta z^{-1}) = (1-\beta z^{-1})B_p(\beta z^{-1}) \tag{16b}$$

where $\beta \in (0,1)$. The design of $\bar{B}_p(\beta z^{-1})$ is based on the damped pole-zero pair principle [7,8], which entertains the advantage of controlled waterbed effect in loop shaping.

Arranging Eq. (15) in the form of polynomial Diophantine equation can yield

$$\bar{B}_p(z^{-1})\frac{1}{M(k)}K(z^{-1}) + z^{-m}B_Q(z^{-1}) = \bar{B}_p(\beta z^{-1}) \tag{17}$$

where $Q(z^{-1}) = B_Q(z^{-1})/\bar{B}_p[\beta z^{-1}]$. The conditions required to guarantee that Eq. (17) has a unique solution are [14]:

(1) $\bar{B}_p(\beta z^{-1})$ is divisible by the greatest common factor of $\bar{B}_p(z^{-1})$ and z^{-m}.
(2) The order of $B_Q(z^{-1})$ plus m is greater than or equal to the order of $\bar{B}_p(z^{-1})$.
(3) The order of $B_Q(z^{-1})$ plus m is equal to the order of $\bar{B}_p(z^{-1})$ plus the order of $K(z^{-1})$.

Since $M(k) \in \mathbb{R}$ ($\mathbb{R}$ is the set of real numbers) and $K(z^{-1})$ is an FIR filter, to solve Eq. (17) we can assume

$$\frac{1}{M(k)}K(z^{-1}) = \bar{k}_0 + \bar{k}_1 z^{-1} + \cdots \bar{k}_{n_k} z^{-n_k} \tag{18}$$

Also, we can assume

$$\bar{B}_p(z^{-1}) = 1 + \bar{b}_{p1}z^{-1} + \cdots + \bar{b}_{p\lambda}z^{-\lambda} \tag{19a}$$

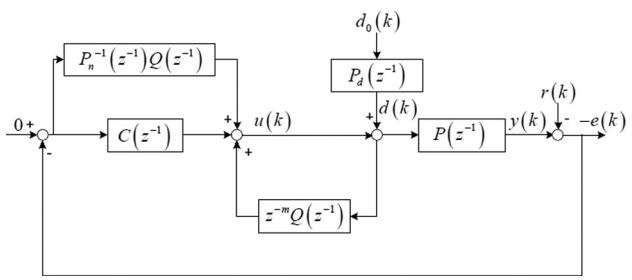

Fig. 2 Loop shaping of DOB

$$\bar{B}_p(\beta z^{-1}) = 1 + \beta\bar{b}_{p1}z^{-1} + \cdots + \beta^{\lambda}\bar{b}_{p\lambda}z^{-\lambda} \tag{19b}$$

According to the conditions mentioned previously, a minimum order solution can be obtained

$$B_Q(z^{-1}) = b_{Q_0} + b_{Q_1}z^{-1} + \cdots + b_{Q_{(\lambda-m)}}z^{-(\lambda-m)} \tag{20}$$

$$\frac{1}{M(k)}K(z^{-1}) = \bar{k}_0 \tag{21}$$

The filter $Q(z^{-1})$ can be determined by equating the respective coefficients of z^{-i} in Eq. (17). In addition, it can be observed that the wind disturbance $M(k)$ will only affect $K(z^{-1})$ but not $Q(z^{-1})$.

3.2 Nonminimum Phase Zeros and Unstable Poles. From Fig. 1, $P_n^{-1}(z^{-1}) \approx z^{-m}P^{-1}(z^{-1})$. $P^{-1}(z^{-1})$ should be stable, in order to ensure the stability of the augmented system. Nevertheless, in most realistic cases, the inverse model of a wind turbine may not be stable. Let the transfer function of the plant be expressed as

$$P(z^{-1}) = \frac{B_p(z^{-1})}{A_p(z^{-1})} \tag{22}$$

where $B_p(z^{-1})$ and $A_p(z^{-1})$ are the numerator and the denominator of $P(z^{-1})$, respectively. When implemented in DOB controller, the roots of polynomial $B_p(z^{-1})$ are the characteristic roots of $P^{-1}(z^{-1})$. They must be inside the unit circle in the z plane, in order to be implementable. If any of the zeros of $P(z^{-1})$ is outside of or on the unit circle, the output of the closed-loop system with DOB controller will oscillate or diverge. In addition, the results will be highly oscillating if the zeros are on the unit circle or close to -1. The zero-phase error tracking (ZPET), which is a stable model-inverse approximation, is adopted to obtain the stable model inversion $P^{-1}(z^{-1})$ approximately when there are nonminimum phase zeros in $P(z^{-1})$ and to keep the output converge [15].

It is also worth noting that the disturbance signal $d_0(k)$ is assumed to be bounded. The operation of a turbine will be terminated to avoid excessive structural loads, if the wind speed exceeds the cut-out wind speed. If $P_d(z^{-1})$ has unstable poles, although $d_0(k)$ is bounded, $d(k)$ will not be bounded after $d_0(k)$ goes through $P_d(z^{-1})$. It will result in divergence of the whole system. Here, we make a slight change of the disturbance dynamics, by moving the unstable poles to the left plane and at the same time keeping the direct current gain of the modified $P_d(z^{-1})$ the same as that of the original $P_d(z^{-1})$. We can therefore ensure that the disturbance entering the plant is bounded.

3.3 Stability Analysis and Robustness Analysis. As mentioned in Sec. 3.1, the Q filter (shown in Eq. (8)) needs to be carefully selected. In this subsection, we focus on the analyses of the stability and robustness of the closed-loop system, which provides the basis for properly selecting Q filter in practice to asymptotically reject the disturbance.

3.3.1 Stability Analysis. Figure 2 illustrates loop shaping based on Fig. 1. The equivalent controller of the augmented scheme from $e(k)$ to $u(k)$ can be expressed as

$$C_{\text{aug}}(z^{-1}) = \frac{C(z^{-1}) + P_n^{-1}(z^{-1})Q(z^{-1})}{1 - z^{-m}Q(z^{-1})} \tag{23}$$

The complementary sensitivity function from $r(k)$ to $y(k)$ is

$$T = G_{r\to y} = \frac{PC_{\text{aug}}}{1 + PC_{\text{aug}}} = \frac{P(C + P_n^{-1}Q)}{1 - z^{-m}Q + PC + PP_n^{-1}Q} \tag{24}$$

In Eq. (24), all z^{-1} notations are omitted for brevity. When there is no plant mismatch between the actual model and the nominal model, we have $P_n^{-1}(z^{-1}) = z^{-m}P^{-1}(z^{-1})$, and therefore

$$G_{r\to y} = \frac{PC_{\text{aug}}}{1+PC_{\text{aug}}} = \frac{PC+1}{1+PC} = 1 \tag{25}$$

One can obtain perfect tracking of reference generator speed when the Q filter is properly selected. The sensitivity function S_0 of the system with the PID controller only is

$$S_0 = \frac{1}{1+PC} \tag{26}$$

Also, the current sensitivity function from $d(k)$ to $e(k)$ is

$$S = \frac{1}{1+PC_{\text{aug}}} = \frac{1-z^{-m}Q}{1+PC+\left(PP_n^{-1}-z^{-m}\right)Q} \tag{27}$$

In frequency regions where the nominal model has a small mismatch with the actual model, we have $PP_n^{-1} - z^{-m} \approx 0$. The frequency response of S will not be significantly influenced by the spectrum of $(PP_n^{-1} - z^{-m})Q$, and thus $S = S_0(1 - z^{-m}Q)$. The sensitivity function performance can be enhanced by the proper selection of Q filter. When Q is stable, the stability of S will be guaranteed [8]. On the other hand, in frequency regions where a large mismatch exists between the linearized reduced-order model and the nonlinear model of the wind turbine, a very small $Q(e^{-j\omega})$ has to be selected to maintain S in the form of $1/(1+PC)$ in order to suppress the disturbance effects through the original PID controller. As the sensitivity function S is only determined by the frequency response of $(1 - z^{-m}Q)$, a large cutoff frequency in Q is desired to reject wider disturbance bandwidth. However, due to physical limitations in hardware and turbine components, the cutoff frequency cannot be very large in practice.

3.3.2 Robustness Analysis. A high-fidelity model of wind turbine requires a very large number of DOFs. The aerodynamic load imposed to the blades is often influenced by the time-varying wind speed, the asymmetric wind shear effect, the tower shadow effect, and the varying azimuth position when the rotor rotates. The dynamics neglected due to order-reduced modeling and the uncertainties/variations of the plant parameters introduce inevitably model mismatch. From the preceding discussion of stability analysis, Q should be carefully selected in frequency regions where there is a mismatch between the nominal model and the actual turbine. The conditions to satisfy the robust stability are discussed in details as follows.

The characteristic polynomial of the closed-loop augmented scheme is given as

$$1 + P(z^{-1})C_{\text{aug}}(z^{-1}) = 0 \tag{28}$$

Let the bounded perturbed model uncertainty from the nominal plant be $\Delta(z^{-1})$. The nominal model is an order-reduced linearized model (under uniform constant 18 m/s wind speed with 5DOFs switched on, as presented Sec. 2). The nonlinear turbine with unmodeled dynamics under time-varying wind speed can be approximately represented as

$$P_r(z^{-1}) = P(z^{-1})(1 + \Delta(z^{-1})) \tag{29}$$

The robust stability condition should be satisfied according to the small gain theorem [16]

$$\|T(e^{-j\omega})\Delta(e^{-j\omega})\|_\infty < 1 \tag{30}$$

T is the complementary sensitivity function in Eq. (24). We can therefore choose the proper cutoff frequency in the Q filter to maintain the stability of the augmented feedback system where there is a model mismatch. In the Q filter, the cutoff frequency can be adjusted by selecting different values of β, and the slope of high frequency response can be further tuned by an extra compensator as will be shown in Sec. 4.

4 Case Analyses and Discussion

In this section, case analyses and comparisons are conducted for both the linearized model and nonlinear plant. First, a 5DOF linearized model of the NREL offshore 5-MW wind turbine is obtained from FAST, and employed to verify preliminarily the effectiveness of the DOB controller. Both uniform stepwise constant and uniform random wind disturbances are used to examine the DOB controller. Then, the DOB controller designed based on the 5DOF linearized model is applied to the nonlinear turbine model and compared with the GSPI controller developed in Ref. [1] (which is treated as the baseline for comparison in nonlinear plant). Based on the robustness analysis presented in Sec. 3.3, we further introduce a compensator to deal with the model mismatch to improve the DOB controller.

4.1 Disturbance Observer Controller Implemented to Linearized Model. To examine the initial design principle and to gain the preliminary understanding of its effectiveness, we first apply a DOB controller to the linearized model. For Q filter formulation, m (the relative degree of $P(z^{-1})$) is 1, and β is chosen to be 0.9953 which can yield the largest disturbance rejection bandwidth and simultaneously guarantee the system convergence. Following the design strategy provided in Sec. 3.1, we can compute, based on Eq. (17), that $Q(z^{-1}) = (0.003609 - 0.0009153\ z^{-1} - 0.009577z^{-2} + 0.008121z^{-3} - 0.00123z^{-4})/(0.3701 - 0.7643z^{-1} + 0.09668z^{-2} + 0.6728z^{-3} - 0.4269z^{-4} + 0.05161z^{-5})$. For comparison purpose, a conventional PID controller is designed, where the proportional (-0.0018225), integral (-0.0040), and derivative (-0.00031894) gains are carefully selected to yield small overshoot and fast settling time. Here, it is worth mentioning that we cannot use the GSPI gains in Ref. [1] because that GSPI controller is designed for nonlinear plant. The stepwise wind disturbance and the corresponding time-domain generator speed error responses of DOB and PID are shown in Figs. 3(*a*) and 3(*b*). It is observed from Fig. 3(*b*) that the DOB has an overshoot of 50 rpm and the PID has an overshoot of 70 rpm. The DOB control leads to a reduction of generator speed error overshoot by 28.57%, while maintaining the same settling time. The frequency-domain reponse under random wind disturbance is presented in Fig. 4. The amplitude spectrum of time-domain results show decrease in frequencies below 1 Hz.

4.2 Disturbance Observer Controller Implemented to Nonlinear Wind Turbine Under Turbulent Wind Field. As shown above, the DOB control with the linearized model exhibits promising performance under stepwise and random disturbances. For the nonlinear plant, the response analysis of the 5-MW benchmark wind turbine is carried out by connecting FAST with the respective controllers in the MATLAB/SIMULINK environment. The time duration is from 0 to 600 s with an integration step of 0.0125 s. All available 16DOFs are turned on, which include:

- first flapwise blade mode (three blades)
- second flapwise blade mode (three blades)
- first edgewise blade mode (three blades)
- drivetrain rotational-flexibility
- generator
- yaw
- first fore–aft tower bending-mode
- second fore–aft tower bending-mode
- first side-to-side tower bending-mode
- second side-to-side tower bending-mode

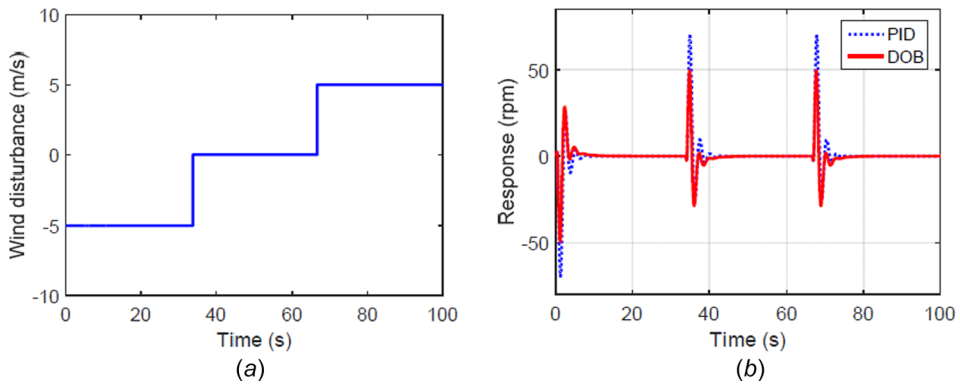

Fig. 3 Wind disturbance and generator speed responses (under 5DOF linearized model): (*a*) stepwise wind disturbance and (*b*) comparison of time-domain responses of DOB and PID

Aerodynamic forces and moments are calculated by using AeroDyn [17]. Realistic turbulent wind fields are generated in TurbSim using IEC Kaimal spectral model [18]. The turbulence intensity (the ratio of root-mean-square (RMS) of the turbulent velocity fluctuations to the mean velocity) is selected as standard IEC category B, which is 14%. Pitch saturation is added to limit the pitch angle between 0 and 90 deg. The pitch rate limiter has a maximum absolute rate of 8 deg/s. The actuator is a first-order model.

First, we directly apply the augmented controller to the nonlinear model to investigate the effectiveness. The PID controller $C(z^{-1})$ is chosen to be the GSPI controller (treated as the baseline) for nonlinear plant. It is worth noting that the model mismatch between the nominal nonlinear turbine and the linearized model in practice will influence the stability of the augmented feedback system. Therefore, the Q filter used in Sec. 4.1 needs to be modified to have a larger β (0.997) to ensure its convergence. From the bode diagram of Q under different β values shown in Fig. 5, the frequency regions which yield $Q = 1$ for $\beta = 0.97$ and $\beta = 0.999$, respectively, are 0.0001–0.3 Hz and 0.0001–0.004 Hz. Consequently, a smaller β gives a wider bandwidth of disturbance rejection since we can achieve perfect disturbance rejection when $Q = 1$. However, a smaller β also leads to a larger magnitude in high frequency region where model mismatch usually happens. According to the stability analysis in Sec. 3.3, a very small $Q(e^{-j\omega})$ is desired to maintain S in the form of $1/(1+PC)$ in model-mismatch frequency regions. It can retain the capability of suppressing disturbance effects of the original GSPI controller and maintain the stability of the augmented system. The nonlinear plant is convergent when $\beta \geq 0.997$. The modification of Q filter can be realized by changing β or even by including an extra compensator (which will be discussed in Sec. 4.3). Here, we first change β to guarantee the stability of the nonlinear system.

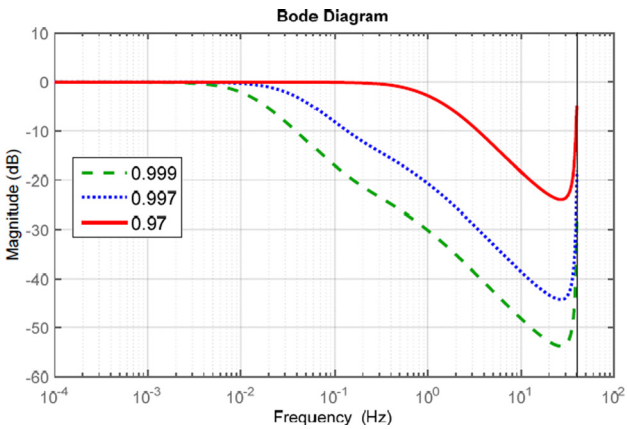

Fig. 5 Bode diagram of *Q* filter under different β

The controller is examined under nine wind files with mean speeds from 14 m/s to 22 m/s. These wind files cover virtually the entire region 3. Figure 6 shows the zoom-in result of generator speed at steady-state between 300 s and 350 s under 18 m/s turbulent wind file. It can be seen that the generator speed stays near the rated value of 1173.7 rpm. Less oscillation around the rated value 1173.7 rpm under DOB control is observed. To quantify the overall speed regulation, RMS errors of generator speed under different turbulent wind files are calculated and listed in Table 1. From Table 1, we can see that the DOB control reduces the RMS

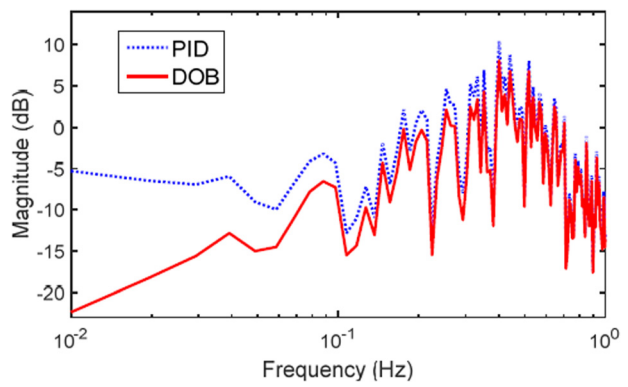

Fig. 4 Frequency-domain generator speed performance comparison of DOB and PID under 5DOF-linearized model and random wind field

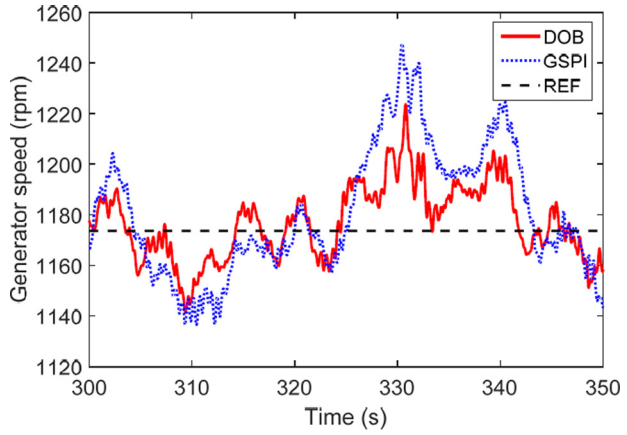

Fig. 6 Zoom-in view of generator speed responses. REF refers to the rated generator speed.

Table 1 Comparisons of generator speed RMS error and power RMS error by GSPI, DOB, and DOB*

Mean wind speed	Controller	Speed RMS error	Power RMS error
14	GSPI	0.0687	0.9506
	DOB	0.0742 (+8.01%)	1.0470 (+10.14%)
	DOB*	0.0448 (−34.79%)	0.6497 (−31.65%)
15	GSPI	0.0782	1.1440
	DOB	0.0825 (+5.50%)	1.1933 (+4.31%)
	DOB*	0.0562 (−28.13%)	0.7844 (−31.43%)
16	GSPI	0.0799	1.2757
	DOB	0.0818 (+2.38%)	1.2387 (−2.90%)
	DOB*	0.0526 (−34.17%)	0.8200 (−35.72%)
17	GSPI	0.0836	1.4124
	DOB	0.0806 (−3.59%)	1.2684 (−10.20%)
	DOB*	0.0530 (−36.60%)	0.8757 (−38.00%)
18	GSPI	0.0879	1.5096
	DOB	0.0831 (−5.46%)	1.3681 (−9.37%)
	DOB*	0.0535 (−39.14%)	0.9042 (−40.10%)
19	GSPI	0.0929	1.6652
	DOB	0.0878 (−5.49%)	1.5072 (−9.49%)
	DOB*	0.0572 (−38.43%)	0.9951 (−40.24%)
20	GSPI	0.0987	1.8439
	DOB	0.0922 (−6.59%)	1.6537 (−10.32%)
	DOB*	0.0610 (−38.20%)	1.0892 (−40.93%)
21	GSPI	0.0991	1.9864
	DOB	0.0906 (−8.58%)	1.7129 (−13.77%)
	DOB*	0.0621 (−37.34%)	1.2351 (−37.82%)
22	GSPI	0.1046	2.1170
	DOB	0.0946 (−9.56%)	1.8125 (−14.38%)
	DOB*	0.0657 (−37.19%)	1.3558 (−35.96%)

errors of speed and power for six wind files, but increases the RMS errors for the other three wind files. Indeed, the modification of Q filter to some extent sacrifices the disturbance rejection capability, as the neglected modes of the plant severely limit the bandwidth of Q filter.

4.3 An Added Compensator Design to Improve Q Filter. As shown in Sec. 4.2, while we can modify the Q filter in the DOB controller by tuning β to guarantee the stability of the nonlinear closed-loop system, the performance of generator speed regulation in the nonlinear plant cannot be guaranteed. Here, we further study the Q filter design in order to deal with the model mismatch between the linearized model and the nonlinear turbine in practice. We prefer smaller magnitude in high frequency region and larger cutoff frequency which are hard to be achieved simultaneously as shown in Fig. 5. To further widen the disturbance rejection region, we propose to add an extra compensator (i.e., a low-pass filter) with faster roll-off at high frequencies. Here, a fourth-order filter $1/(1+\tau s)^4$ is added to tune the high frequency response when $\beta = 0.92$ is used in the Q filter. The improved controller is referred to as the DOB*.

If $PP_n^{-1} - z^{-m} \approx 0$, Eqs. (26) and (27) yield the current sensitivity function as

$$S(e^{-j\omega}) = S_0(z^{-1})(1 - z^{-m}Q(z^{-1}))_{z=e^{j\omega}} \tag{31}$$

Based on Eq. (31), in Fig. 7, we plot the comparison of frequency responses of the sensitivity functions of PID, DOB, and DOB*. Note that P is selected as the model linearized under constant uniform wind speed of 18 m/s. For the sensitivity function formulation of PID, the proportional and integral gains used follow those derived in Ref. [1]. While a family of curves from the frequency responses of the sensitivity function corresponding to different wind speeds can be generated with the added gain scheduled part, for simplicity, we only pick one representative curve from PID, DOB, and DOB* where the gain scheduled part is omitted to compare the controller performances since the performances exhibit similar trend with or without the gain scheduled part. From Fig. 7,

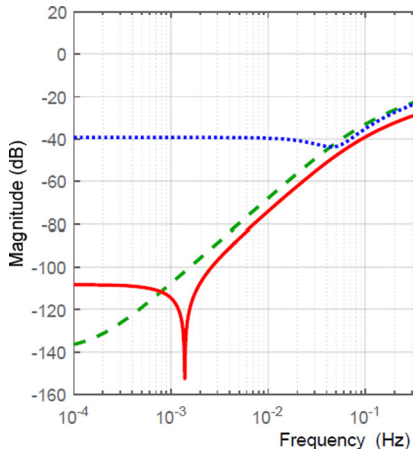

Fig. 7 Comparison of magnitude responses of sensitivity functions

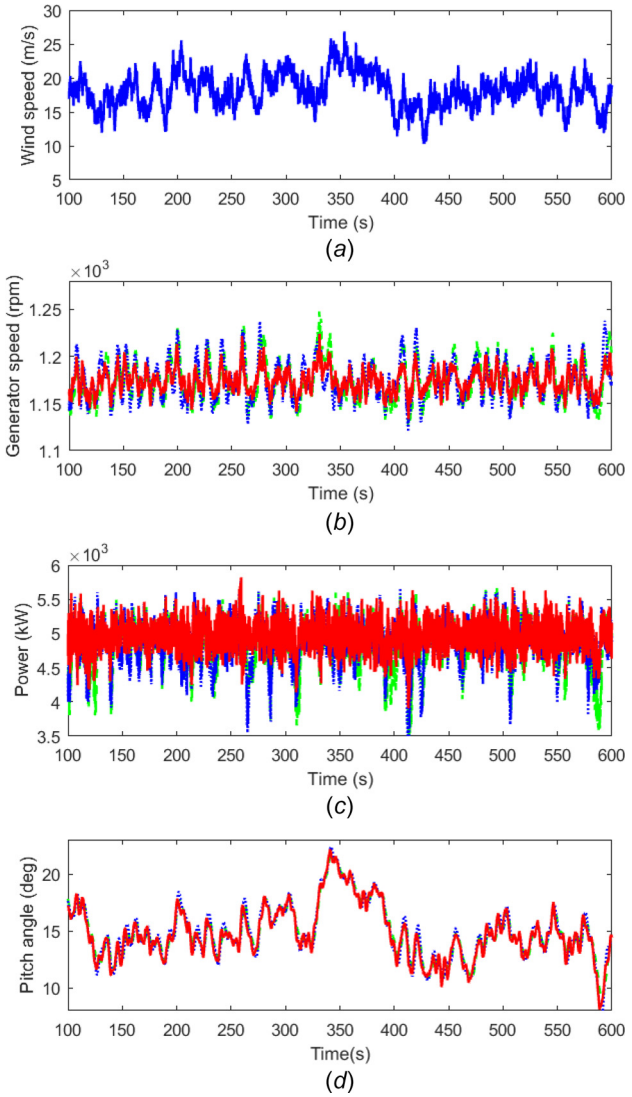

Fig. 8 Time-domain performance comparison of DOB, DOB*, and GSPI: (*a*) wind speed (18 m/s turbulent field), (*b*) generator speed, (*c*) power, and (*d*) pitch angle. - - - -: GSPI, ·····: DOB, ——: DOB*

for the DOB controller formulated based on Sec. 4.2, we can observe magnitude reduction from 0.05 Hz to 1 Hz. Meanwhile, DOB* with an extra compensator yields significant reduction of magnitude from 0.0006 Hz to 2 Hz. The magnitude response of DOB* is smaller compared with both DOB and PID, which indicates that the DOB* can improve considerably the disturbance rejection performance. Figure 8 shows the time-domain responses of wind speed, generator speed, power, and blade pitch angle. With DOB*, generator speed and power response show less fluctuation as compared with the other two controllers, while the pitch angle has more fluctuation which means more pitch activity regulating the generator speed. Figure 9 gives the frequency response comparison of the time-domain data under 18 m/s turbulent wind file, from which we can clearly see the decreased magnitude of DOB* in 0.01–0.16 Hz.

The performance of the DOB* controller is also tabulated in Table 1. The results are obtained under the same nine wind files used in Sec. 4.2. We can observe a decrease in generator speed RMS error by approximately 35% and a similar decrease in power RMS error by approximately 35% compared to those of GSPI. To further facilitate visual comparison of the three controllers, Fig. 10 displays the decreased percentage of generator speed RMS error, where an obvious drop is observed in DOB* (approximately −35%) compared to GSPI.

Finally, we investigate the influences of DOB* on pitch rate, average power capture, and loads on blades, tower, and low-speed shaft. Here, we examine the fatigue damage equivalent load (DEL) which serves as an important metric for comparing fatigue loads across the entire spectrum of turbulent wind files. The equivalent damage is represented by a constant load and calculated by using MLife [19] based on the rainflow counting algorithm. The RMS pitch rate, average power, low-speed shaft torque (LSShftTq) DEL, blade root edgewise moment DEL, blade root flapwise moment DEL, tower base side-to-side moment DEL, and tower base fore–aft moment DEL under nine wind files are shown in Fig. 11. We can observe that the RMS pitch rate is generally increased under DOB* than GSPI, but the controller still works within the pitch rate limit (8 deg/s). The average power in DOB* is increased (+1.18% to +2.74%) compared to GSPI because of the reduction of the power RMS error. The low-speed shaft torque (LSShftTq) DEL values exhibit consistent decrease (−3.65% to −11.02%) for nine wind files because the reduction of fluctuation of rotor speed will directly influence the drive-train torsional load. The blade root edgewise moment DEL values are nearly unchanged (−0.75% to +1.17%) for nine wind files. The blade root flapwise moment DEL values do not change much (−0.29% to +3.56%) except for the one under 14 m/s. The tower base side-to-side moment DEL values increase (+1.57% to +46.49%) for some wind files, but decrease (−3.85% to −20%) for other wind files. The tower base fore–aft moment DEL values increase (+8.64% to +34.04%) for all wind files. It is worth emphasizing that the disturbance observer structure is designed for speed and power regulation and can indeed enhance those performances. On the other hand, the effects to the component loads may be mixed, which is consistent with the results obtained by similar studies [20,21].

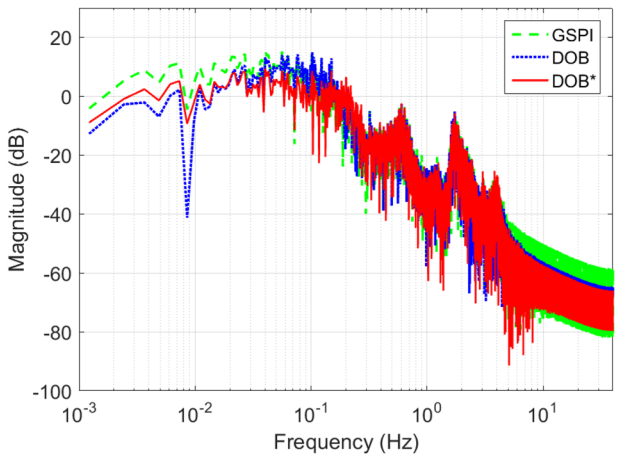

Fig. 9 Frequency-domain performance comparison of DOB, DOB*, and GSPI, under 18 m/s turbulent wind file: (*a*) overall performance and (*b*) zoom-in view at low-frequency region

5 Conclusion and Future Work

In this research, an internal model-based DOB design combined with a PID type feedback controller is formulated for wind turbine generator speed regulation under time-varying unknown wind disturbance. The key idea is to conduct an internal disturbance observation using model inversion and to achieve disturbance cancelation using an inner feedback control loop. The proposed approach is implemented to both the linearized reduced-order model and the nonlinear NREL offshore 5-MW baseline wind turbine model. The DOB controller shows decreased overshoot for the linearized model. To improve the control robustness as it is applied to the nonlinear turbine with inevitable model mismatch between the linearized reduced-order model and actual model

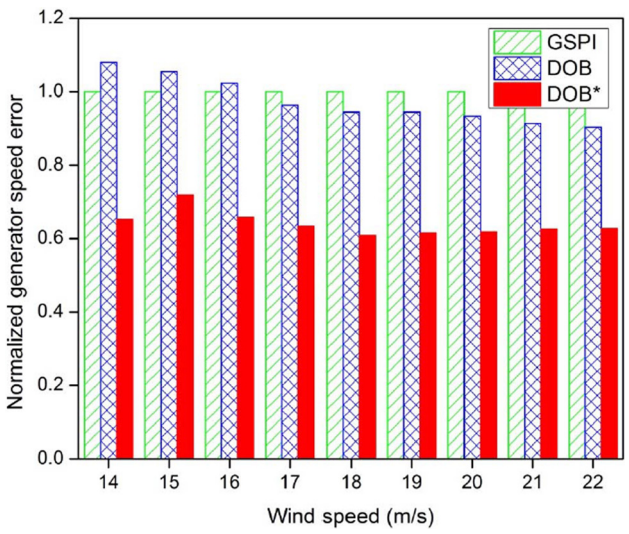

Fig. 10 Generator speed error performance comparison of DOB, DOB*, and GSPI. The generator speed errors of DOB and DOB* are normalized with respect to the error of GSPI.

especially in high frequency regions, design criterion for the Q filter involved is formulated. Furthermore, an extra compensator is introduced to enhance the generator speed regulation. Our case studies indicate that the eventual control strategy, referred to as the DOB* control, can yield approximately 35% reduction in generator speed RMS error and approximately 35% reduction in power RMS error as compared with the PID controller. Since the component loads are not explicitly treated as control objective, the loads on certain components have mixed results.

Future work may include investigating the rejection of periodic wind disturbance which can help to achieve load mitigation on blades and tower in the controller design. Individual pitch control can be explored to mitigate asymmetric blade loads. Online system identification can be used to derive the turbine model to design an adaptive Q filter.

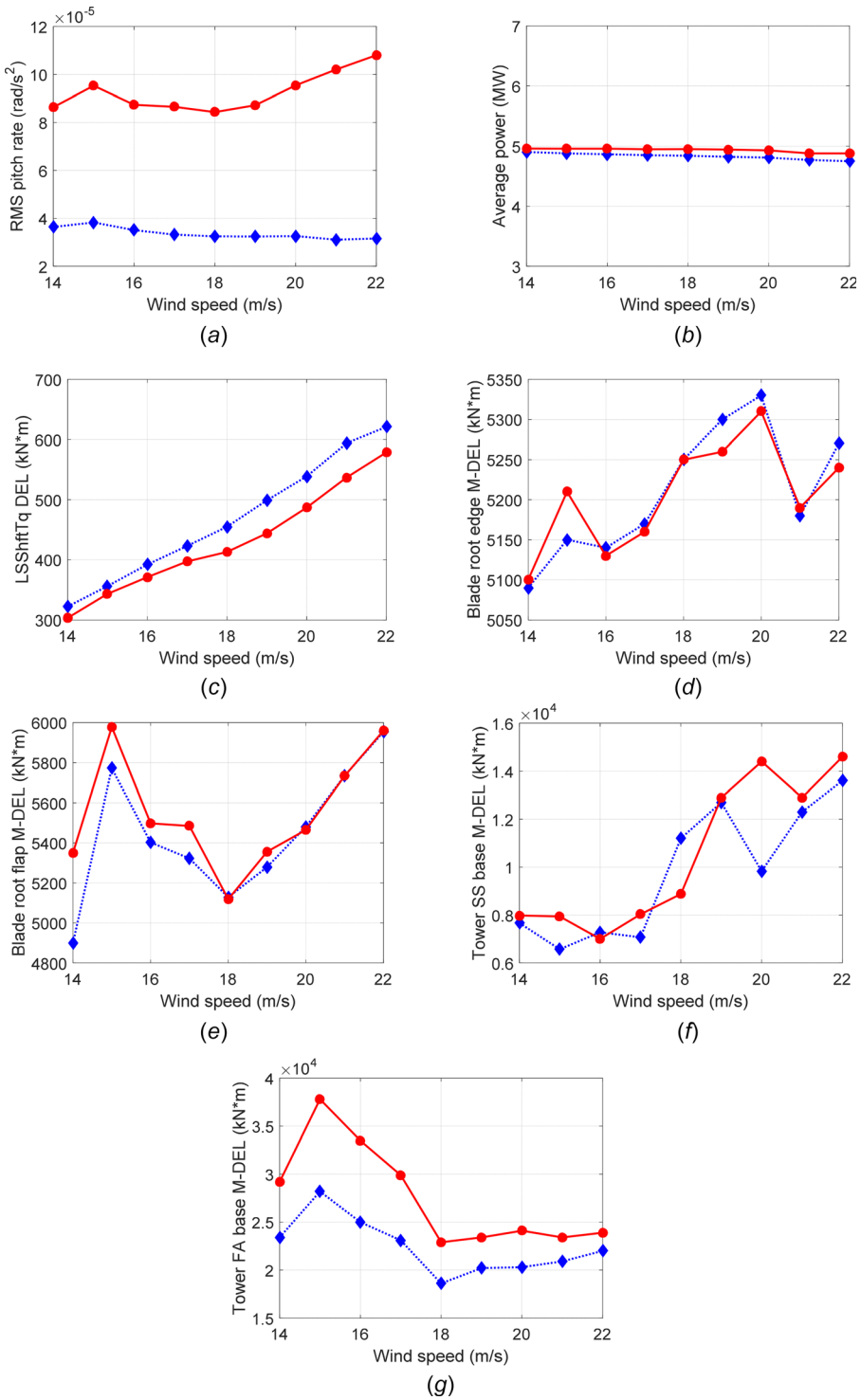

Fig. 11 Comparisons of RMS pitch rate (*a*), average power (*b*), low-speed shaft torque moment DEL (*c*), blade root edgewise moment DEL (*d*), blade root flapwise moment DEL (*e*), tower base side-to-side moment DEL (*f*), and tower base fore–aft moment DEL, and (*g*) of GSPI and DOB*. ---◆---: GSPI, —●—: DOB*

Acknowledgment

This research was supported by National Science Foundation under Grant CMMI–1300236.

References

[1] Jonkman, J. M., Butterfield, S., Musial, W., and Scott, G., 2009, "Definition of a 5-MW Reference Wind Turbine for Offshore System Development," National Renewable Energy Laboratory, Golden, CO, Technical Report No. NREL/TP-500-38060.

[2] Wright, A. D., 2004, "Modern Control Design for Flexible Wind Turbines," National Renewable Energy Laboratory, Golden, CO, Technical Report No. NREL/TP-500-35816.

[3] Wright, A. D., and Balas, M. J., 2003, "Design of State-Space-Based Control Algorithms for Wind Turbine Speed Regulation," ASME J. Sol. Energy Eng., **125**(4), pp. 386–395.

[4] Frost, S. A., Balas, M. J., and Wright, A. D., 2009, "Direct Adaptive Control of a Utility-Scale Wind Turbine for Speed Regulation," Int. J. Robust Nonlinear Control, **19**(1), pp. 59–71.

[5] Wang, N., Johnson, K. E., and Wright, A. D., 2012, "FX-RLS-Based Feedforward Control for LIDAR-Enabled Wind Turbine Load Mitigation," IEEE Trans. Control Syst. Technol., **20**(5), pp. 1212–1222.

[6] Selvam, K., Kanev, S., and van Wingerden, J. W., 2009, "Feedback–Feedforward Individual Pitch Control for Wind Turbine Load Reduction," Int. J. Robust Nonlinear Control, **19**(1), pp. 72–91.

[7] Chen, X., and Tomizuka, M., 2015, "Overview and New Results in Disturbance Observer Based Adaptive Vibration Rejection With Application to Advanced Manufacturing," Int. J. Adapt. Control Signal Process., **29**(11), pp. 1459–1474.

[8] Chen, X., and Tomizuka, M., 2013, "Control Methodologies for Precision Positioning Systems," American Control Conference, Washington, DC, June 17–19, pp. 3704–3711.

[9] Balas, M. J., Magar, K. S. T., and Frost, S. A., 2013, "Adaptive Disturbance Tracking Theory With State Estimation and State Feedback for Region II Control of Large Wind Turbines," American Control Conference, Washington, DC, June 17–19, pp. 2220–2226.

[10] Kempf, C. J., and Kobayashi, S., 1999, "Disturbance Observer and Feedforward Design for a High-Speed Direct-Drive Positioning Table," IEEE Trans. Control Syst. Technol., **7**(5), pp. 513–526.

[11] Laks, J. H., Dunne, F., and Pao, L. Y., 2010, "Feasibility Studies on Disturbance Feedforward Techniques to Improve Load Mitigation Performance," National Renewable Energy Laboratory, Golden, CO, Technical Report No. NREL/SR-5000-48598.

[12] Jonkman, J. M., and Buhl, M. L., Jr., 2005, "FAST User's Guide," National Renewable Energy Laboratory, Golden, CO, Technical Report No. NREL/EL-500-38230.

[13] Francis, B. A., and Wonham, W. M., 1976, "The Internal Model Principle of Control Theory," Automatica, **12**(5), pp. 457–465.

[14] Chen, X., and Tomizuka, M., 2012, "A Minimum Parameter Adaptive Approach for Rejecting Multiple Narrow-Band Disturbances With Application to Hard Disk Drives," IEEE Trans. Control Syst. Technol., **20**(2), pp. 408–415.

[15] Tomizuka, M., 1987, "Zero Phase Error Tracking Algorithm for Digital Control," ASME J. Dyn. Syst. Meas. Control, **109**(1), pp. 65–68.

[16] Doyle, J. C., Francis, B. A., and Tannenbaum, A. R., 1990, *Feedback Control Theory*, Macmillan Publishing Co., New York.

[17] Moriarty, P. J., and Hansen, A. C., 2005, "AeroDyn Theory Manual," National Renewable Energy Laboratory, Golden, CO, Technical Report No. NREL/TP-500-36881.

[18] Jonkman, J. M., 2009, "TurbSim User's Guide: Version 1.50," National Renewable Energy Laboratory, Golden, CO, Technical Report No. NREL/TP-500-46198.

[19] Hayman, G., 2012, "MLife Theory Manual Version 1.00," National Renewable Energy Laboratory, Golden, CO, Technical Report No. NREL/TP-XXXXX.

[20] Dunne, F., Pao, L. Y., Wright, A. D., Jonkman, B., and Kelley, N., 2011, "Adding Feedforward Blade Pitch Control to Standard Feedback Controllers for Load Mitigation in Wind Turbines," Mechatronics, **21**(4), pp. 682–690.

[21] Ma, Z., Shaltout, M. L., and Chen, D., 2015, "An Adaptive Wind Turbine Controller Considering Both the System Performance and Fatigue Loading," ASME J. Dyn. Syst. Meas. Control, **137**(11), p. 111007.